Predictability of mineral dust concentrations: The African Monsoon Multidisciplinary Analysis first short observation period forecasted with CHIMERE-DUST

Laurent Menut, Isabelle Chiapello, Cyril Moulin

Predictability of mineral dust concentrations: The African Monsoon Multidisciplinary Analysis first short observation period forecasted with CHIMERE-DUST

Laurent Menut,[1] Isabelle Chiapello,[2] and Cyril Moulin[3]

Received 2 June 2008; revised 28 October 2008; accepted 29 January 2009; published 2 April 2009.

[1] The predictability of northern Africa dust events is assessed using daily numerical forecast simulations for the next 3 days. The dust concentration fields, modeled with the CHIMERE-DUST model, were first evaluated by comparison with both Aerosol Robotic Network (AERONET) surface data and Ozone Monitoring Instrument (OMI) and Spinning Enhanced Visible and Infrared Imager (SEVIRI) satellite measurements. The accuracy and spread between measurements and simulations are discussed for the first short observation period of the African Monsoon Multidisciplinary Analysis (AMMA) experiment in western Africa, between January and March 2006. The predictability of dust events was then estimated by comparing model results for different leads in a forecast mode. The model performance was evaluated with respect to its capability to forecast the surface wind speed, which is the key process for dust emission, and the transport of mineral dust near source regions and toward remote areas. It is shown that forecast emissions can vary up to 80% (close to the sources) but that the variability on forecasted dust concentrations and optical thicknesses do not exceed 40% and 20%.

Citation: Menut, L., I. Chiapello, and C. Moulin (2009), Predictability of mineral dust concentrations: The African Monsoon Multidisciplinary Analysis first short observation period forecasted with CHIMERE-DUST, *J. Geophys. Res.*, *114*, D07202, doi:10.1029/2008JD010523.

1. Introduction

[2] Mineral dust emitted in arid and semiarid areas strongly affect the biogeochemical cycles [e.g., *Jickells et al.*, 2005] and the Earth radiative budget [e.g., *Sokolik et al.*, 2001]. The assessment of these impacts requires to use dedicated three-dimensional transport models to obtain regional or global dust concentrations fields.

[3] These models are used in several contexts, from the study of specific dust events of a few days during field experiments [e.g., *Myhre et al.*, 2003; *Bouet et al.*, 2007], to the study of the global impact of dust on climate [*Miller and Tegen*, 1998]. The modeling of mineral dust often focusses on the understanding of the most outstanding dust events [*Tulet et al.*, 2008] because they cause considerable damages on environment and health. On the contrary, such models are rarely used for the daily forecast of dust events [*Grini et al.*, 2006]. The sporadic character of dust events is linked to the emission process, which is strongly dependent on surface characteristics. For a given location, the intensity of the emission depends on the so-called saltation threshold. For wind speed below this threshold, no dust is emitted. When the wind speed increases, the intensity of emissions evolves nonlinearly. For moderate wind speed, dust emissions are weak but can lead to significant background dust concentrations because of their regularity. For very high wind speed such as those observed during intense dust events, huge dust emissions occur in a few hours.

[4] The model capability to properly simulate a dust event is directly linked to the accuracy of the computed saltation threshold velocity. In addition to the accuracy on the wind speed, the surface characteristics, which are never perfectly reproduced, also play an important role in the simulation of dust emissions. Indeed, even for an uncertainty of a few meters per second on the surface wind speed, most models ensure realistic emissions for intense dust events because the wind speed is much larger than the saltation threshold. Modeling problems occur at lower wind speed because the system becomes very sensitive to the absolute wind speed value.

[5] Modeling extreme dust events is thus much easier than modeling the day-to-day evolution of the background dust concentration. In a forecast context, it is mandatory to account for all dust events, light or strong. Near sources, semipermanent background dust concentrations may lead to environment and health damages similar or even greater than those of sporadic intense dust events. The daily forecast of atmospheric dust concentration is thus the main

[1] Institut Pierre-Simon Laplace, Laboratoire de Météorologie Dynamique, Ecole Polytechnique, Palaiseau, France.
[2] Laboratoire d'Optique Atmospherique, Université des Sciences et Technologies de Lille, CNRS, Villeneuve d'Asce, France.
[3] Institut Pierre-Simon Laplace, Laboratoire des Sciences du Climat et de l'Environnement, CEA Orme des Merisiers, Gif sur Yvette, France.

0148-0227/09/2008JD010523

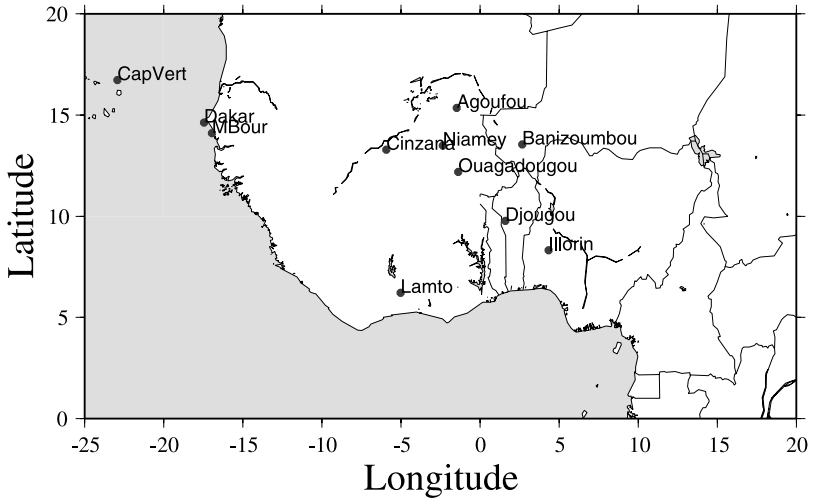

Figure 1. Map of the main AERONET stations used in this study.

challenge for modelers. Several systems are currently used for the forecast of mineral dust such as the regional DREAM model in Barcelona (http://www.bsc.es/projects/earthscience/), the SKIRON system (http://forecast.uoa.gr/dustindx.php) and the global NRL model (http://www.nrlmry.navy.mil/aerosol/).

[6] In this paper, we present dust forecast results obtained with the CHIMERE-DUST model for a domain covering North Africa, North Atlantic and western Europe between January and March 2006. This period corresponds to the first short observation period of the African Monsoon Multidisciplinary Analysis (AMMA) international field campaign [*Redelsperger et al.*, 2006]. For each forecasted day, modeled dust concentrations were first compared to satellite and ground-based measurements. In order to quantify the differences between model and observations in terms of forecast variability, dust concentrations were then compared for the same time with several forecast leads. On the basis of the studied 3-month period, the relative part of the forecast variability (and associated uncertainty) on the model performance is quantified and discussed.

2. The AMMA Experiment

2.1. Overview of the AMMA Program and Observational Strategy

[7] AMMA is a coordinated international project dedicated to improve the knowledge of the West African monsoon and its variability on daily to interannual timescales [*Redelsperger et al.*, 2006]. A major goal of AMMA was to progress in the understanding of the regional and global influence of the West African monsoon on the physical, chemical, and biological environment. Another key aspect of this project was to use multidisciplinary researches to relate climate variability to issues on health, water resources, food security and demography for West African nations. The African continent being the largest source of mineral dust, these aerosols play a major role in radiative forcing and cloud microphysics and thus are an important component of the West African monsoon system. The AMMA observations program relies on a multiscale approach both spatially, from local to regional and global scales, and temporally, with three defined observational periods: the long-term observing period (LOP, 2001–2010); the enhanced observing period (EOP, 2005–2007), and the Special Observing Period (SOP: 2006). The SOP focuses on the four main phases of the monsoon cycle: (1) the dry season (SOP0, January-February), (2) the monsoon onset (SOP1, May-June), (3) the well developed monsoon (SOP2, July-August), and (4) the late monsoon (SOP3, August-September).

2.2. AEROSOL Measurements During AMMA

2.2.1. Ground-Based Measurements

[8] Biomass burning occurs during the winter dry season (November-February) over the Sahelian region, whereas mineral dust events are observed all year long over western Africa, with significant seasonal changes in intensity and transport pattern [*Chiapello et al.*, 1995]. The main objective of the SOP0 experiment performed in January-February 2006 was to characterize the physical, chemical, and optical properties as well as the radiative effect of both biomass burning and desert dust particles [*Haywood et al.*, 2008]. Another aspect of the SOP0 was to use the deployed measurements to validate and improve numerical models (global and regional) of these two aerosol species in order to better understand their impacts on radiation budget, hydrological cycle and climate. In this context, a wide observational network has been established, especially for aerosol characterization. The experimental strategy relied on the reinforcement of the western Africa surface sites with Sun photometers installed on a semipermanent basis as part as the Aerosol Robotic Network (AERONET) [*Holben et al.*, 2001]. In addition, four sites were fully equipped with in situ and remote sensing instruments, such as lidar, radiometers, cascade impactors, particle counters, and filter samples for aerosol chemistry analysis. These sites were defined as the AMMA super sites. The sites of Banizoumbou (Niger) and Tamanrasset (Algeria) were focused on mineral dust, whereas the site of Djougou (Benin) was more influenced by biomass burning aerosols and that of M'Bour (Senegal) was dedicated to the characterization of the mixture of dust and biomass burning (Figure 1). In this study, we used Sun photometer data acquired in the AMMA

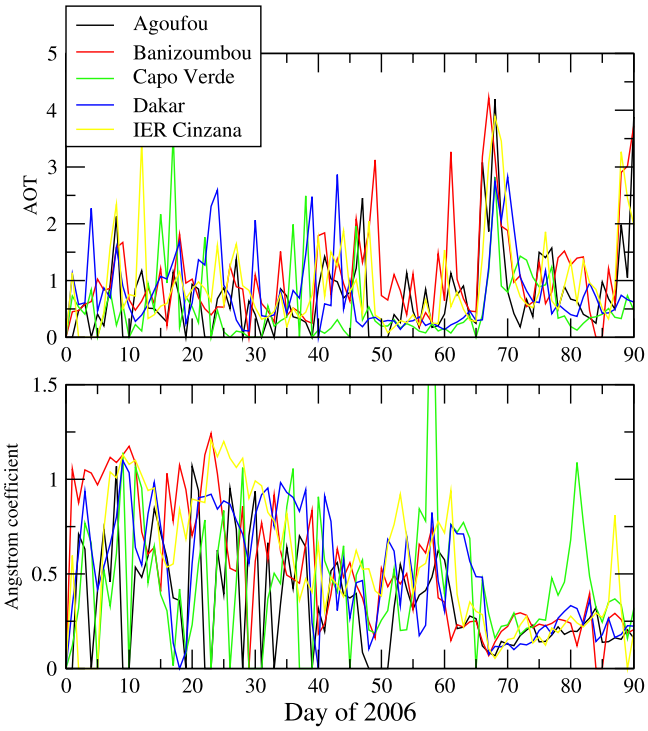

Figure 2. Daily evolution of AOT (440 nm) and Angström coefficient (440–675 nm) measured during the period January-March 2006 for the AERONET stations. The strongest AOT peaks, occurring on Julian days 68, 69, and 70 (8, 9, and 10 March 2006) correspond to the lowest values of Angström coefficients, indicating a pure dust event.

context at Djougou (Benin), Banizoumbou (Niger), Agoufou (Mali), Cinzana (Mali), M'Bour (Senegal) and Sal Island (Cape Verde). Note that except for the site of Djougou, all these stations are located along an east-west transect of dust emissions and transport toward the northeastern tropical Atlantic.

[9] Figure 2 shows the daily evolution of the aerosol optical thickness (AOT, at 440 nm) and Angström coefficient (440–675 nm) measured from January to March 2006 at AERONET sites located along the east-west transect of dust. These measurements show that the most intense aerosol peak during the period was in March 2006, with AOT higher than 2 at all stations and was associated with low Angström coefficients (i.e.,<0.2), which indicate the presence of large particles of mineral dust. It is remarkable that this major dust storm was recorded at all the ground-based stations from the easternmost site in Niger to the westernmost one in Cape Verde Islands, with maximum AOT occurring between 8 March (Banizoumbou) and 10 March (Cinzana). Other high AOT events were recorded during January and February 2006, but they were weaker and shorter than the event of March. Moreover, in most cases the associated Angström coefficients were relatively high, indicating that aerosols contain a significant fraction of small biomass burning particles. Specific aerosol analysis performed at M'Bour confirms the influence of both mineral dust and biomass burning aerosol in January-February and the presence of pure mineral dust in March [*Derimian et al.*, 2008; *Heese and Wiegner*, 2008].

2.2.2. Satellite Observations

[10] In order to evaluate the spatial distribution of dust simulated by CHIMERE-DUST, the recently developed aerosol product derived from Meteosat Second Generation (MSG)/Spinning Enhanced Visible and Infrared Imager (SEVIRI) observations was used. The inversion technique developed by *Thieuleux et al.* [2005] allows retrieval of both aerosol optical thickness (AOT at 0.55 nm), and Angström coefficient using SEVIRI measurements at 0.63 and 0.81 nm. A preliminary validation from *Thieuleux et al.* [2005] has shown that these two aerosol products are in good agreement with AERONET ground-based measurements. One limitation is that these MSG/SEVIRI retrievals are available only over oceanic regions surrounding Africa, i.e., the Atlantic Ocean and the Mediterranean Sea. Despite this limitation, this aerosol product is particularly suitable to monitor North African dust transport because of its temporal resolution of 15 min. In the context of AMMA, SEVIRI aerosol products were generated by Interactions Clouds Aerosols Radiations (ICARE) for the year 2006 and made available at two spatial resolutions (3 km and 12 km). For 2006, the only available satellite dust product covering both oceanic surfaces and arid regions of North Africa is the Ozone Monitoring Instrument (OMI) aerosol index (AI). OMI, on board the Aura platform launched in 2004 as part of the A-Train, may be considered as the successor of Total Ozone Mapping Spectrometer (TOMS) which was efficient to infer desert dust variability over both land and ocean [*Chiapello et al.*, 1999; *Chiapello and Moulin*, 2002; *Moulin and Chiapello*, 2004]. The aerosol index product initially developed by *Herman et al.* [1997] and *Torres et al.* [1998] for the TOMS sensors is only a semiquantitative product which suffers from some limitations, especially from a dependency to the altitude of the aerosol layer and from a low spatial resolution (here we use the 1° in latitude and 1.25° in longitude grid). Another disadvantage is that the AI detects both mineral dust and biomass burning particles, without any possible distinction between the two aerosol species. For all these reasons the OMI AI product should be used with caution. An overview of the OMI aerosol products, description of the algorithms and summary of validation results are presented by *Torres et al.* [2007].

3. The CHIMERE-DUST Model

3.1. Main Model Characteristics

[11] The model consists of three elements: (1) the meteorological platform with the MM5 model forced by the National Centers for Environmental Prediction (NCEP) global meteorological fields, (2) the dust emissions model, (3) the CHIMERE-DUST transport model. These elements are used together and in the same manner in both analysis and forecast modes.

[12] The horizontal analysis data of NCEP [*Kalnay et al.*, 1996] are provided on a regular 1.125° × 1.125° grid. These fields are used as boundary conditions and nudging for the MM5 model [*Dudhia*, 1993].

[13] The dust emissions scheme used in the model is the *Marticorena and Bergametti* [1995] scheme. It computes

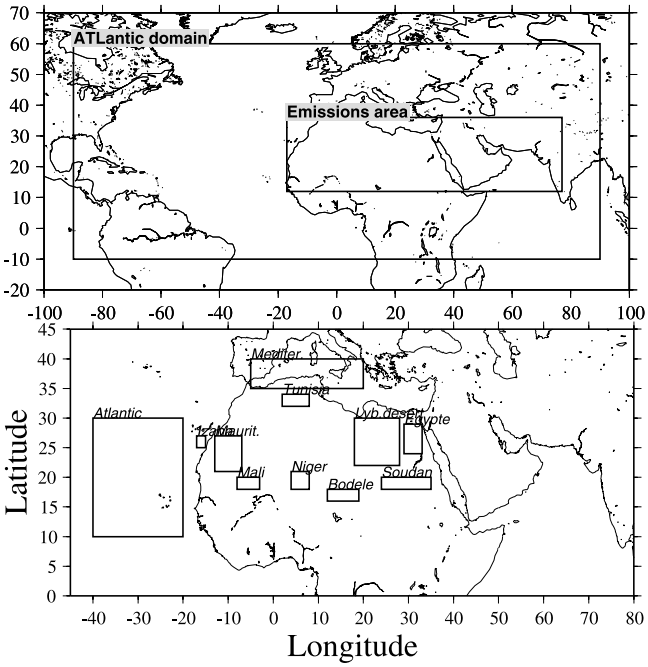

Figure 3. (top) Map of the CHIMERE-DUST simulation domains. The "ATL" domain used in this study extended from $\lambda = -90°$W to $\lambda = +90°$E and from $\phi = -10°$S to $\phi = +60°$N. The domain where the potential dust emissions are diagnosed is noted "emissions area". (bottom) The selected areas used for comparisons.

horizontal fluxes from wind velocities and surface features for the emissions area ("emissions" area in Figure 3).

[14] The dust vertical fluxes are computed using the *Alfaro and Gomes* [2001] parameterization, optimized following *Menut et al.* [2005]. This parameterization defines flux distributions for three main tabulated particles diameters which depend on the surface characteristics and on the soil texture. The estimated three fluxes are then redistributed into the model size bins using a mass partition scheme. The wet deposition scheme is that described by *Loosmore and Cederwall* [2004]. The dry deposition velocity is parameterized following *Venkatram and Pleim* [1999].

[15] The dust transport model CHIMERE-DUST was developed on the basis of the chemistry-transport model CHIMERE [*Vautard et al.*, 2001; *Bessagnet et al.*, 2004]. The horizontal domain has a horizontal grid resolution of $1° \times 1°$ and is displayed as the "ATL" frame in Figure 3. Vertically, 15 levels are defined from the surface to 200 hPa. Turbulent parameters as, u_*, the friction velocity and, $\overline{h}$, the boundary layer depth are estimated from the mean meteorological parameters (the wind components, u and v, the temperature T, the specific humidity q, and the pressure p). The horizontal transport is performed using the Van Leer scheme [*Van Leer*, 1979], the vertical transport with the first-order upwind scheme and the vertical mixing is estimated from the calculation of the bulk Richardson number as extensively described by *Menut* [2003]. There is no added numerical horizontal diffusion considering that the transport scheme is diffusive enough. The dust simulations are performed with a time step of 7 min and 30 s.

[16] In order to compare the modeled dust to surface network data, the concentrations are vertically integrated and converted into AOT (using Mie theory and extinction coefficients calculated for the wavelengths of the AERONET measurements used for comparisons, after [*Moulin et al.*, 1997]).

3.2. Forecast Model Setup

[17] The CHIMERE-DUST model used for forecast is strictly the same than the version used for analysis or sensitivity studies. The meteorological fields used to drive CHIMERE-DUST are issued from the NCEP forecast fields (same structure as those described by *Kalnay et al.* [1996]. Every day, around midnight, the meteorological fields are downloaded for a period ranging from midnight of the day before, called [D - 1] (the analysis period, including data assimilation performed by NCEP) to 3-day forecast, called [D + 3]. These fields are used to run the CHIMERE-DUST model. Each day, dust concentrations are calculated during fours days: from the day before to 3 days in advance as presented in Figure 4. For example, for 12 March 2006, modeled data range from 11 March 2006, 0000 UTC ([D - 1]) to 14 March 2006, 2300 UTC ([D + 3]). Forecast fields are provided on a Web site every morning (http://www.lmd.

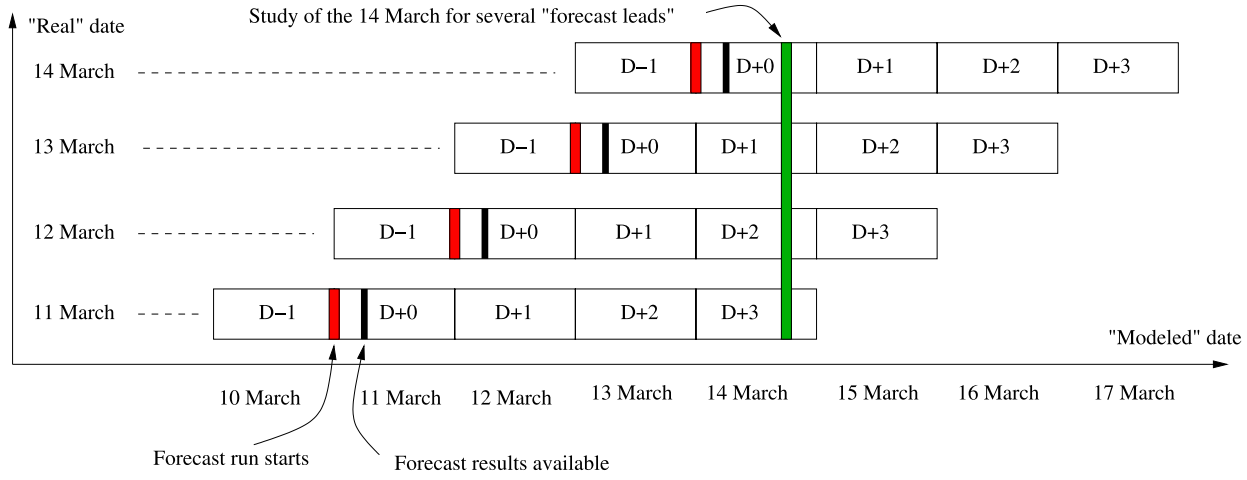

Figure 4. Principle of the CHIMERE-DUST forecast modeling system.

polytechnique.fr/dust). The dust initial conditions are issued from the CHIMERE-DUST forecast done the day before.

4. Comparisons Between Measurements and Simulations

4.1. Horizontal Patterns

[18] Figure 5 compares the OMI AI and the SEVIRI AOT to the modeled AOT. Three examples are presented, first short observation period (SOP0). These examples were chosen only to show the capability of the model to simulate large-scale dust plumes and their temporal evolution.

[19] Satellites products were projected onto the model grid ($1^\circ \times 1^\circ$) in order to facilitate the comparison. For 10 February, a relatively weak dust event is observed, which occurred in the center of Africa and with limited spatial extension. OMI recorded two local maxima of AI, also predicted by CHIMERE-DUST. For 25 February, an intense dust plume occurred in the vicinity of the Bodélé depression, whereas a second dust plume is recorded on the eastern side of the Mediterranean sea. High values are also diagnosed with SEVIRI and correspond to the large dust plume modeled with CHIMERE-DUST. An example of an intense dust event occurred on 10 March with dust coming from the center of Africa and being transported eastward across the Atlantic Ocean. The simulated plume has the same horizontal extension and location than the one observed with satellite data. In addition, the measured (SEVIRI) and modeled AOT are very close, with maxima values of about 2. Overall, these comparisons show that for different cases, the satellite data and the model outputs agree very well in terms of aerosol occurrences as well as of plume shapes and intensities.

4.2. AOT Time Series

[20] The focus of this section is on the AOT evolution for selected areas. Using SEVIRI data and CHIMERE-DUST model outputs, AOT is averaged over predefined areas: the ''Atlantic Ocean'' and the ''Mediterranean Sea'' as defined in Figure 3 (bottom). With SEVIRI, data are only available over ocean, restricting the comparison to these areas. The results are presented in Figure 6 as time series of spatially averaged AOT between 1 January and 20 March 2006. For the two areas, SEVIRI values are always higher than the model results. This is the direct impact of a measurement that sums up all aerosols in the atmosphere (biomass burning, anthropogenic emissions, sea salts and mineral dust) while the model only accounts for mineral dust. As found by *Thieuleux et al.* [2005], the uncertainty induced by the algorithm delivering AOT over oceans from measured radiances may be a few tenths. In addition, sea salt may induce a relatively high and homogeneous background, recorded by the satellite but not taken into account in CHIMERE-DUST. In this case, it is difficult to conclude on the model ability to retrieve the satellite value since this is in the uncertainty range. Over the Atlantic Ocean, a background value of mineral dust leading to an AOT of about 0.1 is modeled while a total background value of AOT $\approx$ 0.25 is observed with SEVIRI. Because of deposition processes during long-range transport, the values are lower over the Mediterranean Sea: the averaged background value for modeled dust is close to zero, whereas the SEVIRI total aerosol retrieval is around 0.15. For the specific event of 8–12 March 2006, clearly identified as a pure dust event (Figure 2), the measured and modeled AOT are very close over the Atlantic Ocean.

5. Model Input Data and Forecast Dust Variability

5.1. Spread of Meteorological Forecast

[21] In this section, we evaluate the ''spread'' of the meteorological forecast which represents the degree of agreement between various forecast leads. The most sensitive meteorological parameter for dust emissions is the surface wind speed [*Menut*, 2008]. Since the emission scheme was elaborated using the 10 m wind speed, $|U|_{10m}$, we compare forecasted time series with wind speeds measured at different sites.

[22] In Figure 7, modeled wind speed are presented for Djougou and Dakar as examples, for the first 10 days of March 2006, when the highest dust events were observed. For one specific date, several values are reported corresponding to different ''leads'' (from [D − 1] to [D + 2]). The forecast lead is the time between the last available analysis concentrations field and the studied forecast concentrations field. For example, the forecast lead called [D + 2] corresponds to the second day after the analysis data of [D + 0].

[23] The forecast spread increases with the difference between the values because of the uncertainty on the wind speed forecast. In Djougou, the wind speed remains low with values below 5 m s^{-1}. Some peaks up to 6 m s^{-1} are modeled for some leads only, leading to fluctuating estimates of dust emissions. In M'Bour, at the coastline, the wind speed was obviously higher. This location was not a dust source but in the way of the major transport from land to ocean. Thus the forecast variability will have an impact on the transport of dust over the Ocean and on its spatial structure. For the two sites, and for wind speed values ranging from 2 to 6 m s^{-1}, the forecast variability from [D − 0] to [D + 2] may reach ±2 m s^{-1}: this means that over dust sources or during long-range transport, the forecast may have an error of up to 100% for low values (not very crucial for emissions) and up to 30% for highest wind speed values.

5.2. Spread of Dust Emissions Forecast

[24] The significant spread estimated for the wind speed has a direct impact on dust emissions estimated with the model. Because of the threshold characteristics of the saltation and sandblasting processes, an error on the wind speed may decide whether dust is generated or not for a specific location and a specific time. Figure 8 presents an example of surface emission fluxes (in g cm^{-2} d^{-1}), calculated with the dust production model and over the western Africa. The two maps represent the same place and time for two different leads: emissions are estimated for 1 March 2006 and integrated over the whole day. Results for 1 March are taken from model runs started on 2 March ([D − 1]) and on 26 February ([D + 3]). The [D − 1] results represent the best fluxes since it was estimated using the reanalyzed wind fields (including the data assimilation process). The spread is very large and showed that 3 days in advance, the dust emissions fluxes are much more important than the day before using the analyzed wind

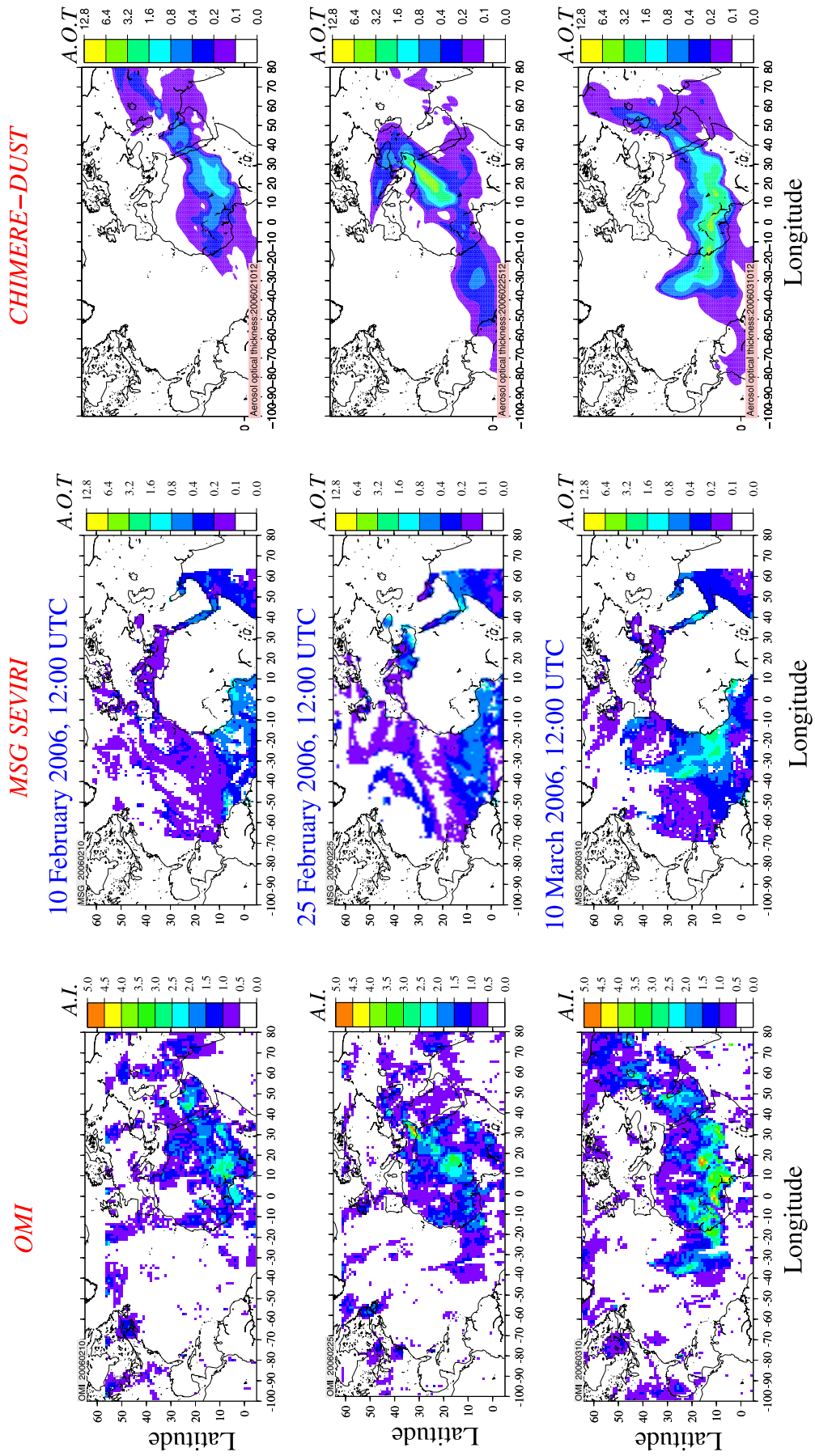

Figure 5. Maps of (left) aerosol index with OMI, [middle] optical thickness by SEVIRI and (right) modeled aerosol optical thickness, for 10 February, 25 February, and 10 March 2006, 1200 UTC.

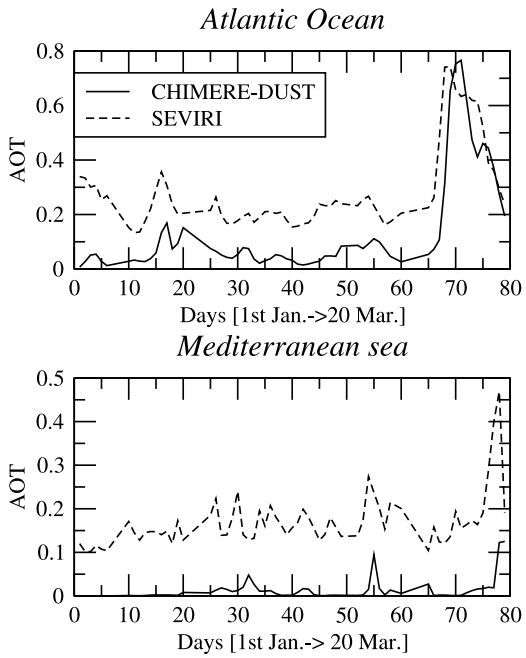

Figure 6. Comparison of aerosol optical thickness recorded by SEVIRI and modeled by CHIMERE-DUST during the first 3 months of 2006 and over two specific areas: Atlantic Ocean and Mediterranean Sea as displayed in Figure 3.

fields. In this case, overestimated wind speeds associated with the threshold process of dust emission lead to a spread of a factor of 3 to 4 on dust emission fluxes for some parts of the domain. The analysis of these changes is difficult because the effects are not spatially homogeneous.

5.2.1. Dust Surface Concentrations Forecast Variability

[25] The coupled impact of the forecast variability of wind speed and of dust emissions is quantified using the surface dust concentrations modeled with CHIMERE-DUST. Figure 9 presents surface dust concentration time series for selected sites: Banizoumbou, M'Bour, Djougou, Cinzana in western Africa, Cape Verde in the Atlantic Ocean and Rome in Europe. The results are not displayed with the same timescale in order to focus on the most significant dust event. For all sites in Africa (except Djougou), the higher dust concentrations are estimated for the farthest proceeded forecast. This tendency is clear since maximal concentrations can vary from 2000 to 3000 μg m^{-3} in Banizoumbou or from 2500 to 4500 μg m^{-3} in M'Bour, which corresponds to a forecast overestimation of more than 100%. Over remote sites, as Cape Verde and Rome, it clearly appears that the spread is not regular in time: while some days exhibit a dust variability of more than 100% (day 79 in Rome, for example), some others are very stable for the forecast (day 80 also in Rome). Compared to the European air quality standards the spread in dust forecast (up to 40 μg m^{-3}) is considerable. Therefore, the current state of regional dust forecast is unsatisfying.

5.2.2. Aerosol Optical Thickness Forecast Variability

[26] Results are presented in Figure 10 for the whole SOP0 period and for the same sites than in Figure 9. In addition to errors on modeled wind speeds and emissions, the conversion to AOT adds new potential errors related to the estimation of the dust size distribution. These additional uncertainties in the forecast could increase the potential variability and errors in the results compared to the AERONET data. Surprisingly, the spread of AOT is less clear between the different leads that it was for concentrations: this may be the impact of the modeled dust size distribution times the extinction coefficient for a specific wavelength.

[27] Figure 11 presents the dust concentrations as a function of the bins used in the model: 12 bins ranging from 0.1 μm to 40 μm. The sites are the same than in Figure 10, and the results are presented for the 10 March 2006. For the sites located near dust sources, two modes are clearly present: a fine mode ($D_p \approx 1$ μm) and a coarse mode ($D_p \approx 8$ μm). The highest variability is observed for the fine mode, but also exists for the coarse mode, mainly for sites near sources such as Djougou, M'Bour, and Cinzana. For the M'Bour site, this modeled size distribution is in accordance with the experimental results of *Derimian et al.* [2008].

[28] Even if the variability of the coarse mode is lowest, its contribution to the total mass is preponderant. For the wavelength used to estimate the AOT, the maximum value of the efficient extinction coefficient is for a particle diameter of 0.5 μm. Compared to the dust concentrations in Figure 11, this corresponds to a size bin with a relatively low concentration variability: the peak of concentration varies as a function of the forecast lead but not for the most optically efficient part of extinction coefficient profile. This explains the fact that dust concentrations can have similar errors than AOT but with a larger variability.

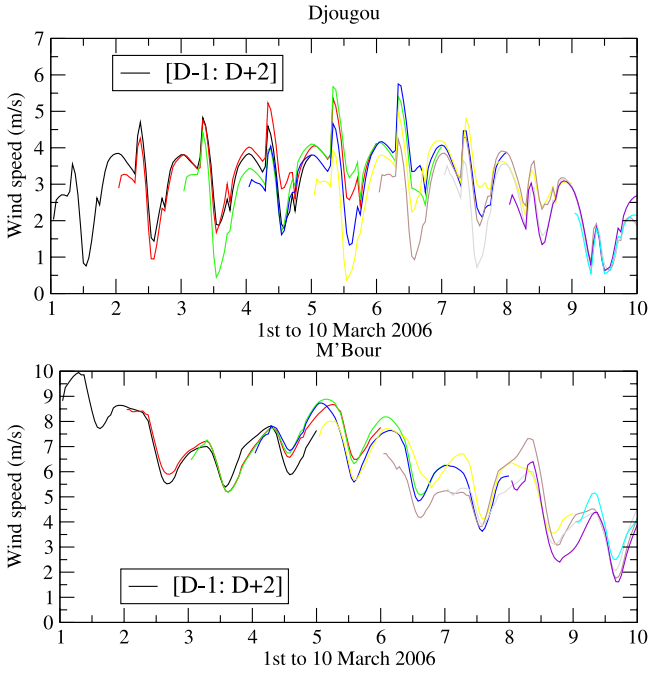

Figure 7. The 10 m wind speed modeled by the NCEP/MM5 model and for each forecast lead. The time series are for the model cells corresponding to the Djougou and Dakar sites and for March 2006. The legend with the black curve is an example of a 5-day time series: this is the same principle for all colored curves.

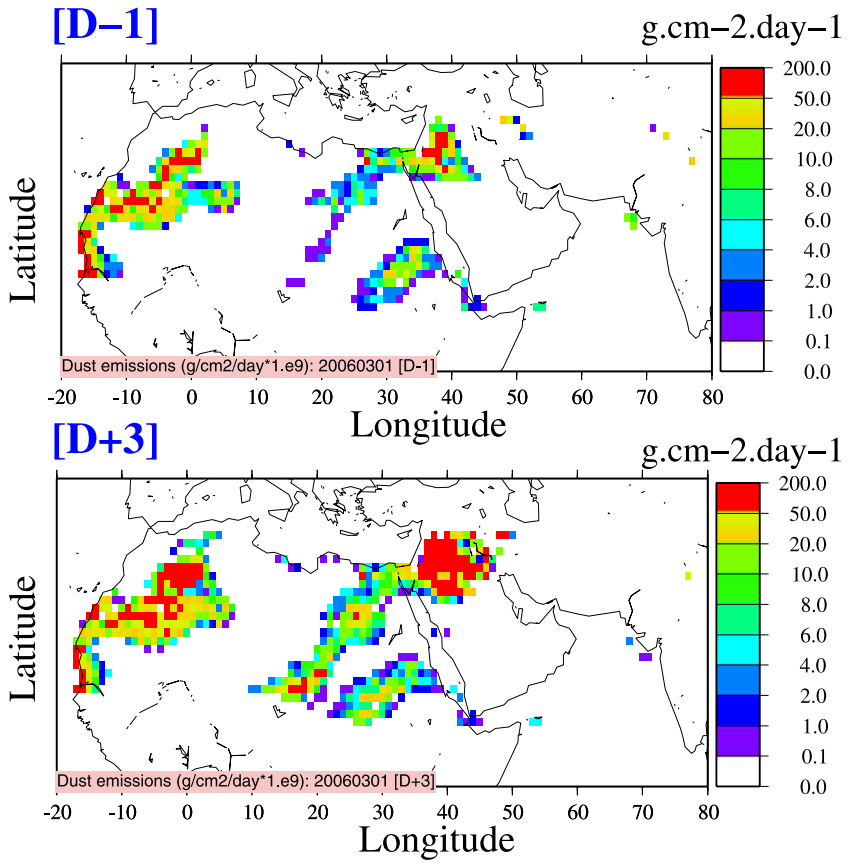

Figure 8. Daily integrated dust emissions fluxes (g cm^{-2} d^{-1}) from different leads ([D − 1] and [D + 3]) on 1 March 2006.

[29] For remote sites such as Rome, measured AOT are higher than model results. This is due to the fact that the model calculates dust emissions only over western Africa (due to its spatially restricted emissions inventory). The long-range transport of dust is responsible for a fraction of the locally measured aerosol optical thickness compared to locally emitted aerosols (traffic, industry). If we consider that the model gives realistic results (in analysis mode), an additional information can be deduced here: the difference between the modeled and the measured AOT can be attributed to the locally emitted dust. During the studied period, the local contribution may reach 50% of the total recorded AOT.

5.3. Forecasted Dust Scores

[30] The results previously discussed for selected sites and periods are finally displayed as forecast scores in the Table 1. For each parameter (surface emission flux, dust load, surface concentration and AOT), the results are averaged over areas defined in Figure 3. In order to estimate the spread of the forecast as a function of time, the ratios of model results for the first day (D-1, i.e., the day of the calculation using the analyzed wind fields) to the results for the studied day are presented.

[31] The value of this ratio increases with the time period between two leads. For example, if the ratio [D + 2]/[D −1] is equal to 1.5, this means that the calculated parameter was 50% higher when forecasted 3 days in advance than the parameter calculated the current day. For the major part of all scores, values are logically increasing, representing error accumulations. Some exceptions are however shown, highlighting the fact that meteorological forecast may drastically change from one day to the next. For the sites in Africa, the tendency is to have increasing scores for surface emissions: this means that the wind speed is systematically overestimated compared to the analyzed values. This is observed for the whole "emissions area," with errors reaching 8% for emissions and 4% on dust concentrations, dust load and AOT. Results are much more variable for zooms in emission areas such as "Bodélé," "Niger," "Mali-Mauritania," and "Mauritania WS" (WS for west-south part of), "Soudan": the last lead has always errors larger than the first one (there is no stabilization of the forecast with time) and larger errors may reach values of 85% as in Bodélé, for example, for emissions. For Bodélé, this leads to a spread of 26% in dust load and 42% and 18% for surface concentrations and AOT, respectively.

[32] Far from these sources, in the northern part of Africa (Egypt, Lybian desert, Tunisia) and in the Canary Islands (Izana), the scores can be underestimated or overestimated. In Egypt, for example, the spread reaches 40% for emissions but very low values for surface concentrations (−7%) and finally gives a spread of 0% for AOT.

[33] This case clearly demonstrates that the errors on emissions may strongly affect the size distribution in mass. This is less significant for the surface concentration scores

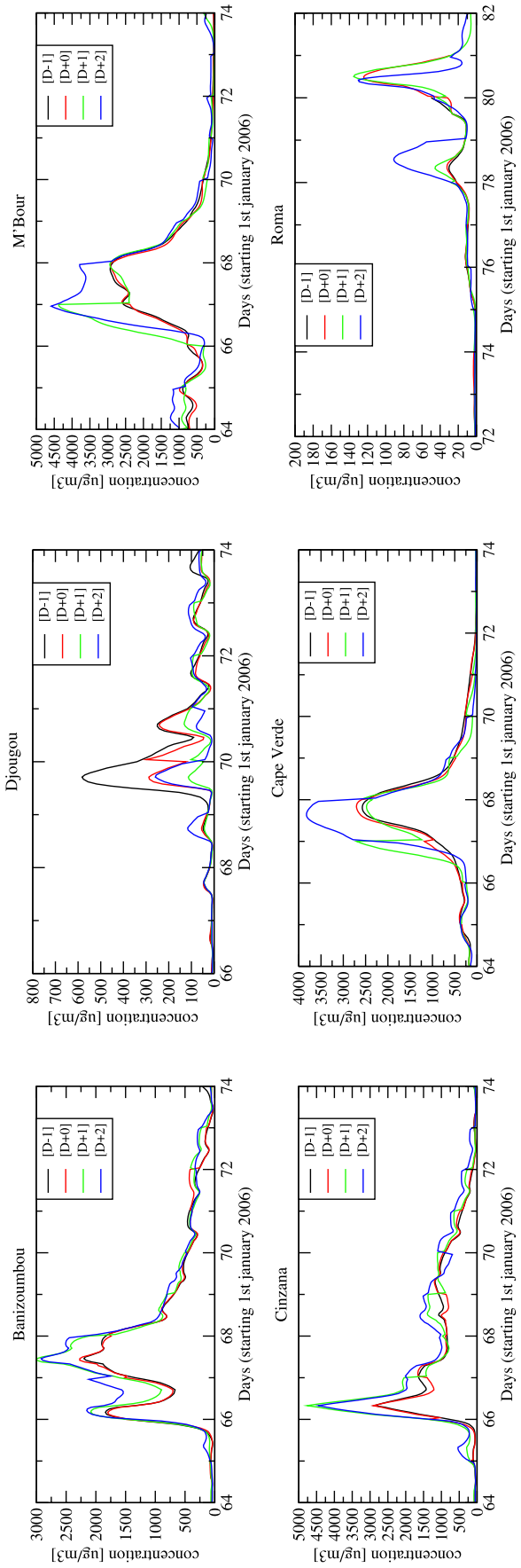

Figure 9. Time series of surface dust concentrations for African (Banizoumbou and Djougou) and European (Rome and Barcelona) sites. For each lead, concentrations values are joined from day to day. The timescale is not the same in order to focus on the most significant event of the period (depending on the location).

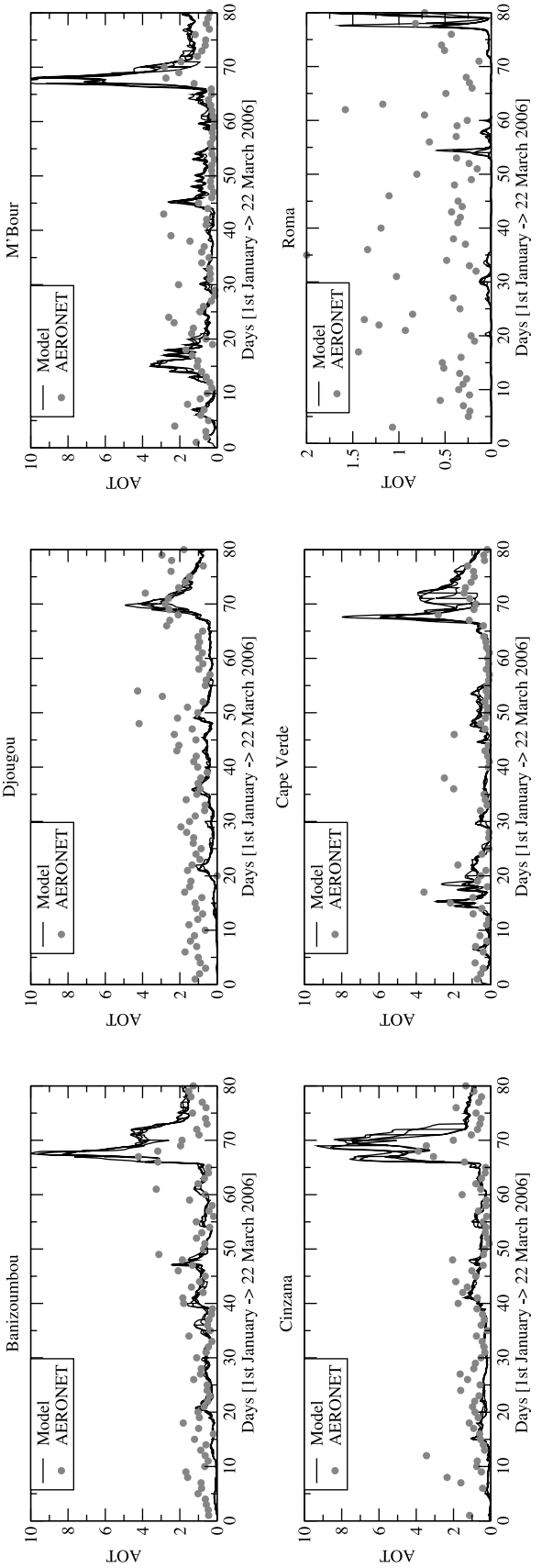

Figure 10. Time series of aerosol optical thicknesses modeled (all leads are superimposed) and recorded by the AERONET Sun photometers network (symbols) during the SOP0 period (from 1 January to 22 March 2006.)

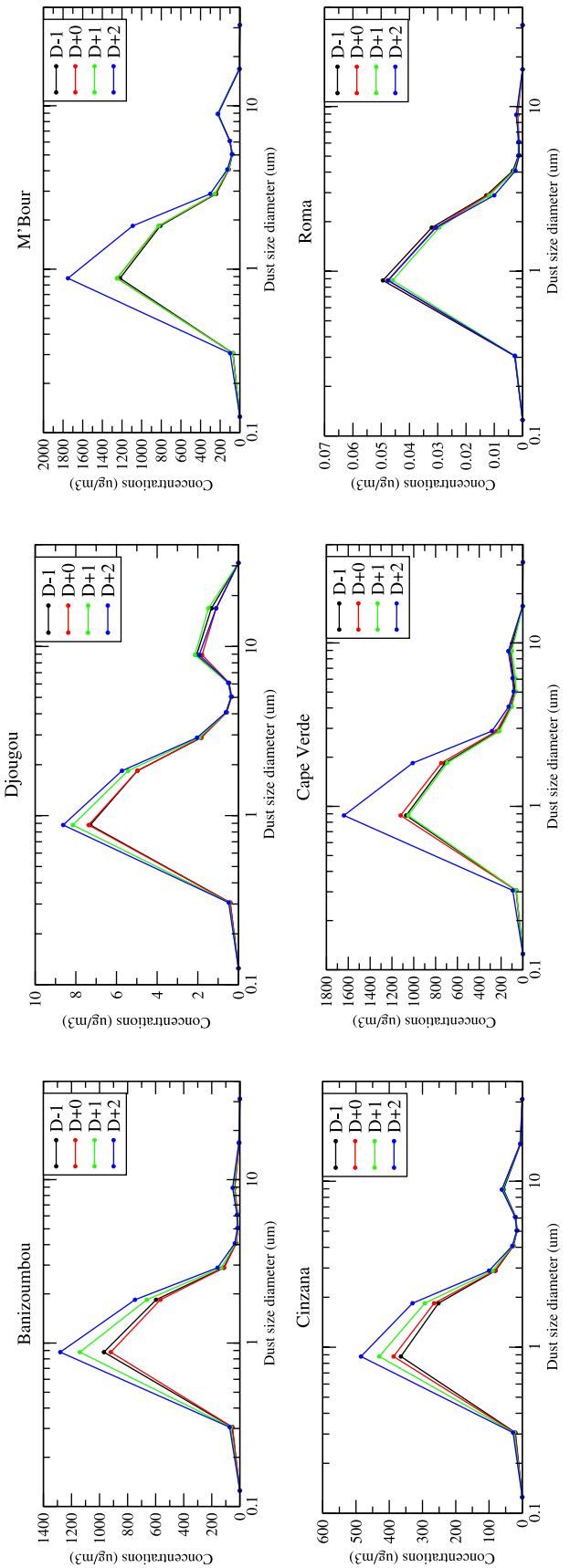

Figure 11. Dust size distribution (μg m^{-3}) for selected sites and for 10 March 2006, 1200 UTC.

Table 1. Dust Emissions Fluxes, Dust Load, and Surface Concentrations Ratios Integrated Over the Whole Period 1 January to 20 March 2007 and Over Specific Restricted Areas[a]

	Surface Emissions			Dust Load			Surface Concentration			AOT		
Site	$\frac{D+0}{D-1}$	$\frac{D+1}{D-1}$	$\frac{D+2}{D-1}$	$\frac{D+0}{D-1}$	$\frac{D+1}{D-1}$	$\frac{D+2}{D-1}$	$\frac{D+0}{D-1}$	$\frac{D+1}{D-1}$	$\frac{D+2}{D-1}$	$\frac{D+0}{D-1}$	$\frac{D+1}{D-1}$	$\frac{D+2}{D-1}$
Emissions area	1.01	1.05	1.08	1.01	1.02	1.04	1.03	1.04	1.04	1.01	1.03	1.04
Bodélé	1.43	1.61	1.85	1.11	1.18	1.26	1.23	1.31	1.42	1.07	1.15	1.18
Niger	1.13	1.25	1.16	1.08	1.21	1.26	1.19	1.39	1.34	1.10	1.19	1.23
Mali-Maur.	1.19	1.33	1.26	1.11	1.09	1.09	1.18	1.10	1.15	1.07	1.08	1.10
Maur. WS	0.92	0.93	0.97	0.94	0.89	0.90	0.94	0.91	0.94	1.02	0.98	0.91
Soudan	1.17	1.19	1.41	1.03	1.04	1.04	1.06	1.09	1.07	1.03	1.07	1.07
Egypt	1.01	1.29	1.40	0.98	1.01	0.97	0.98	0.98	0.93	1.00	1.00	1.00
Lybian Desert	0.94	0.96	0.94	0.94	0.97	0.95	0.99	1.03	0.97	0.97	0.97	0.91
Tunisia	1.19	1.06	1.15	0.76	0.97	0.90	0.86	1.07	0.99	0.74	0.89	0.77
Izana	0.86	0.72	0.79	0.98	1.08	0.98	0.93	0.93	0.87	0.92	0.92	0.90
Atlantic area				1.01	1.02	1.03	1.00	1.01	1.04	1.02	1.03	1.04
Med. area	1.14	0.88	0.78	0.93	0.88	0.87	0.85	0.77	0.89	0.96	0.91	0.89

[a]See map in Figure 3. Maur., Mauritania; Med., Mediterranean.

owing to fast deposition of the coarse particles. Since the optically active part of the size distribution (the fine particles) has a higher residence time in the atmosphere, the AOT appears to be less variable than the total emitted mass or the surface concentration.

[34] Interestingly, in Tunisia the scores do not evolve similarly from day to day: the spread decreases from the first to the second forecast day and increases from the second to the third. This leads to oscillating scores of surface concentrations and AOT. In this case, the wind speed variability associated with possible wind direction changes with leads shows that forecast becomes very uncertain far away from the main sources.

[35] Over the Atlantic Ocean, very stable scores are derived with spread never exceeding 4%: in this case, the forecast of the meteorology is certainly sufficiently stable to ensure a low variability of dust plumes transport. This is not the case for the Mediterranean area, where the scores are higher. In contrast to the Atlantic Ocean (downwind the African dust sources), this area is smaller, and after long-range transport of dust across various land types, the scores are higher. Finally, the more intense spread is always on dust emissions. The dust load and dust surface concentrations followed the same tendency of spread than emissions but to a lesser extent. This aspect is related to a larger error in the emissions of the coarsest particles. They are first emitted by the wind but quickly deposited and thus not accounted for in the budget of surface concentration and dust load. Because of the dust size distribution, with a maximum of particles in the fine mode ($D_p \approx 1$ μm), and the shape of the efficient extinction coefficient (with a maximum at $D_p \approx 0.5$ μm), the spread of AOT remains lower than the one of dust concentration.

6. Conclusion

[36] From January to March 2006, the first short observation period SOP0 of the AMMA experiment was performed in western Africa. In this study, we first analyzed this period by comparing surface stations and satellite measurements to dust concentrations fields of the transport model CHIMERE-DUST. In January and February, aerosols were dominated by biomass burning particles, whereas a huge dust event occurred in early March.

[37] This analysis showed that the model is able (1) to simulate the correct timing of dust emissions over West Africa, with a hourly temporal resolution, and (2) to properly predict the shape and intensity of the dust plume transported from Africa toward the Atlantic Ocean in March 2006.

[38] After the analysis of this 3-month period used for model validation, we focused on the accuracy of the model in a forecast mode. The CHIMERE-DUST model was operated during this SOP0 as a help for the experimental setup (mainly as alert tool for measurements). The goal was to estimate the spread of the daily dust forecast at a regional scale up to 3 days in advance. We showed that the very high spatial and temporal variability of the wind speed forecast prevents from extracting an unique and constant tendency in the forecast scores over the whole model area. Depending on the region and on the meteorological situation, a variability of up to 80% was observed for dust emission fluxes over specific areas, such as the Bodélé area. This led to an averaged variability of about 40% for dust concentrations in western Africa. After long-range transport, the spread reached 40 μg m^{-3} in the south of Europe, which is larger than the required accuracy for air quality forecast. This shows that this regional dust model may be used with a good confidence for hourly emissions and long-range dust transport, but that some improvements are still required to reach current air quality criteria for surface concentrations forecast in western Europe, far away from sources.

[39] The main lacks concern (1) the accuracy of the mean wind speed used to estimate surface emission fluxes, (2) the model ability to represent the long-range transport of thin but very dense layers, and (3) the ability of regional models to correctly estimate the daily mixing convection, responsible of the reintegration of mineral dust into the boundary layer [*Colette et al.*, 2008]. At local scale, some additional improvements would be necessary to better represent local resuspension of already present mineral or terrigenous material. This means a more accurate representation of soil and surface characteristics in the regional models used for forecast in Europe, as in the work by *Honoré et al.* [2008].

[40] **Acknowledgments.** We thank the AERONET/PHOTONS group and AMMA African sites team for the data used in this article.

References

Alfaro, S. C., and L. Gomes (2001), Modeling mineral aerosol production by wind erosion: Emission intensities and aerosol size distribution in source areas, *J. Geophys. Res.*, *106*, 18,075–18,084.

Bessagnet, B., A. Hodzic, R. Vautard, M. Beekmann, S. Cheinet, C. Honoré, C. Liousse, and L. Rouil (2004), Aerosol modeling with CHIMERE—Preliminary evaluation at the continental scale, *Atmos. Environ.*, *38*, 2803–2817, doi:10.1016/j.atmosenv.2004.02.034.

Bouet, C., G. Cautenet, R. Washington, M. C. Todd, B. Laurent, B. Marticorena, and G. Bergametti (2007), Mesoscale modeling of aeolian dust emission during the BoDEx 2005 experiment, *Geophys. Res. Lett.*, *34*, L07812, doi:10.1029/2006GL029184.

Chiapello, I., and C. Moulin (2002), TOMS and Meteosat satellite records of the variability of Saharan dust transport over the Atlantic during the last two decades (1979–1997), *Geophys. Res. Lett.*, *29*(8), 1176, doi:10.1029/2001GL013767.

Chiapello, I., G. Bergametti, L. Gomes, B. Chatenet, F. Dulac, J. Pimenta, and E. S. Suares (1995), An additional low layer transport of Sahelian and Saharan dust over the north-eastern tropical Atlantic, *Geophys. Res. Lett.*, *22*(23), 3191–3194, doi:10.1029/95GL03313.

Chiapello, I., J. M. Prospero, J. Herman, and C. Hsu (1999), Detection of mineral dust over the North Atlantic Ocean and Africa with the Nimbus 7 TOMS, *J. Geophys. Res.*, *104*, 9277–9291, doi:10.1029/1998JD200083.

Colette, A., L. Menut, M. Haeffelin, and Y. Morille (2008), Impact of the transport of aerosols from the free troposphere towards the boundary layer on the air quality in the Paris area, *Atmos. Environ.*, *42*(2), 390–402, doi:10.1016/j.atmosenv.2007.09.044.

Derimian, Y., J.-F. Léon, O. Dubovik, I. Chiapello, D. Tanré, A. Sinyuk, F. Auriol, T. Podvin, G. Brogniez, and B. N. Holben (2008), Radiative properties of aerosol mixture observed during the dry season 2006 over M'Bour, Senegal (African Monsoon Multidisciplinary Analysis campaign), *J. Geophys. Res.*, *113*, D00C09, doi:10.1029/2008JD009904.

Dudhia, J. (1993), A nonhydrostatic version of the Penn State/NCAR mesoscale model: Validation tests and simulation of an Atlantic cyclone and cold front, *Mon. Weather Rev.*, *121*, 1493–1513.

Grini, A., P. Tulet, and L. Gomes (2006), Dusty weather forecasts using the MesoNH mesoscale atmospheric model, *J. Geophys. Res.*, *111*, D19205, doi:10.1029/2005JD007007.

Haywood, J. M., et al. (2008), Overview of the Dust and Biomass-burning Experiment and African Monsoon Multidisciplinary Analysis Special Observing Period-0, *J. Geophys. Res.*, *113*, D00C17, doi:10.1029/2008JD010077.

Heese, B., and M. Wiegner (2008), Vertical aerosol profiles from Raman polarization lidar observations during the dry season AMMA field campaign, *J. Geophys. Res.*, *113*, D00C11, doi:10.1029/2007JD009487.

Herman, J. R., P. K. Bhartia, O. Torres, C. Hsu, C. Seftor, and E. Celarier (1997), Global distribution of UV-absorbing aerosols from Nimbus 7/TOMS data, *J. Geophys. Res.*, *102*(D14), 16,911–16,922, doi:10.1029/96JD03680.

Holben, B. N., et al. (2001), An emerging ground-based aerosol climatology: Aerosol optical depth from AERONET, *J. Geophys. Res.*, *106*(D11), 12,067–12,097.

Honoré, C., et al. (2008), Predictability of European air quality: Assessment of 3 years of operational forecasts and analyses by the PREV'AIR system, *J. Geophys. Res.*, *113*, D04301, doi:10.1029/2007JD008761.

Jickells, T. D., et al. (2005), Global iron connections: Between desert dust, ocean biogeochemistry and climate, *Science*, *308*, 67–71, doi:10.1126/science.1105959.

Kalnay, E., et al. (1996), The NCEP/NCAR 40-year reanalysis project, *Bull. Am. Meteorol. Soc.*, 437–471.

Loosmore, G., and R. Cederwall (2004), Precipitation scavenging of atmospheric aerosols for emergency response applications: Testing an updated model with new real-time data, *Atmos. Environ.*, *38*, 993–1003.

Marticorena, B., and G. Bergametti (1995), Modeling the atmospheric dust cycle: 1. Design of a soil-derived dust emission scheme, *J. Geophys. Res.*, *100*(D8), 16,415–16,430, doi:10.1029/95JD00690.

Menut, L. (2003), Adjoint modeling for atmospheric pollution process sensitivity at regional scale, *J. Geophys. Res.*, *108*(D17), 8562, doi:10.1029/2002JD002549.

Menut, L. (2008), Sensitivity of hourly Saharan dust emissions to NCEP and ECMWF modeled wind speed, *J. Geophys. Res.*, *113*, D16201, doi:10.1029/2007JD009522.

Menut, L., C. Schmechtig, and B. Marticorena (2005), Sensitivity of the sandblasting fluxes calculations to the soil size distribution accuracy, *J. Atmos. Oceanic Technol.*, *22*(12), 1875–1884.

Miller, R., and I. Tegen (1998), Climate response to soil dust aerosols, *J. Clim.*, *11*(12), 3247–3267, doi:10.1175/1520-0442(1998)011<3247:CRTSDA>2.0.CO;2.

Moulin, C., and I. Chiapello (2004), Evidence of the control of summer atmospheric transport of African dust over the Atlantic by Sahel sources from TOMS satellites (1979–2000), *Geophys. Res. Lett.*, *31*, L02107, doi:10.1029/2003GL018931.

Moulin, C., F. Guillard, F. Dulac, and C. E. Lambert (1997), Long-term daily monitoring of Saharan dust load over ocean using Meteosat ISCCP-B2 data 1. Methodology and preliminary results for 1983-1994 in the Mediterranean, *J. Geophys. Res.*, *102*(D14), 16,947–16,958, doi:10.1029/96JD02620.

Myhre, G., A. Grini, J. M. Haywood, F. Stordal, B. Chatenet, D. Tanré, J. K. Sundet, and I. S. A. Isaksen (2003), Modeling the radiative impact of mineral dust during the Saharan Dust Experiment (SHADE) campaign, *J. Geophys. Res.*, *108*(D18), 8579, doi:10.1029/2002JD002566.

Redelsperger, J.-C., C. D. Thorncroft, A. Diedhiou, T. Lebel, D. J. Parker, and J. Polcher (2006), African Monsoon Multidisciplinary Analysis: An international research project and field campaign, *Bull. Am. Meteorol. Soc.*, *87*(12), 1739–1746, doi:10.1175/BAMS-87-12-1739.

Sokolik, I. N., D. M. Winker, G. Bergametti, D. A. Gillette, G. Carmichael, Y. J. Kaufman, L. Gomes, L. Schuetz, and J. E. Penner (2001), Introduction to special section: Outstanding problems in quantifying the radiative impacts of mineral dust, *J. Geophys. Res.*, *106*(D16), 18,015–18,027, doi:10.1029/2000JD900498.

Thieuleux, F., C. Moulin, F. Breon, F. Maignan, J. Poitou, and D. Tanré (2005), Remote sensing of aerosols over the oceans using MSG/SEVIRI imagery, *Ann. Geophys.*, *23*, 3561–3568, doi:1432-0576/ag/2005-23-3561.

Torres, O., P. K. Bhartia, J. R. Herman, Z. Ahmad, and J. Gleason (1998), Derivation of aerosol properties from satellite measurements of backscattered ultraviolet radiation: Theoretical basis, *J. Geophys. Res.*, *103*(D14), 17,099–17,110.

Torres, O., A. Tanskanen, B. Veihelmann, C. Ahn, R. Braak, P. K. Bhartia, P. Veefkind, and P. Levelt (2007), Aerosols and surface UV products from Ozone Monitoring Instrument observations: An overview, *J. Geophys. Res.*, *112*, D24S47, doi:10.1029/2007JD008809.

Tulet, P., M. Mallet, V. Pont, J. Pelon, and A. Boone (2008), The 7-13 March 2006 dust storm over West Africa: Generation, transport, and vertical stratification, *J. Geophys. Res.*, *113*, D00C08, doi:10.1029/2008JD009871.

Van Leer, B. (1979), Towards the ultimate conservative difference scheme. V A second order sequel to Godunov's method, *J. Comput. Phys.*, *32*, 101–136.

Vautard, R., M. Beekmann, J. Roux, and D. Gombert (2001), Validation of a hybrid forecasting system for the ozone concentrations over the Paris area, *Atmos. Environ.*, *35*, 2449–2461.

Venkatram, A., and J. Pleim (1999), The electrical analogy does not apply to modeling dry deposition of particles, *Atmos. Environ.*, *33*, 3075–3076.

I. Chiapello, Laboratoire d'Optique Atmospherique, Université des Sciences et Technologies de Lille, CNRS, F-59655 Villeneuve d'Asce CEDEX, France.

L. Menut, IPSL, Laboratoire de Météorologie Dynamique, Ecole Polytechnique, 61 avenue du Gal De Gaulle, F-91190 Palaiseau, France. (menut@lmd.polytechnique.fr)

C. Moulin, Institut Pierre-Simon Laplace, Laboratoire des Sciences du Climat et de l'Environnement, CEA Orme des Merisiers, Batiment 712, F-91191 Gif-Sur-Yvette, France.